Chapter 5
Catalytic Reforming of CH_4 with CO_2 in a Membrane Reactor: A Study on Effect of Pressure

5.1. Introduction

In this chapter, a membrane reactor study on the CH_4 reforming with CO_2 is presented. The catalytic reforming of CH_4 with CO_2 (Eq. 5.1) was carried out in a hydrogen separation membrane reactor (MR) and a packed bed reactor (PBR) at various pressures (1-20 atm) and temperatures (873 K and 923 K).

$$CH_4 + CO_2 \rightleftharpoons 2CO + 2H_2 \qquad \Delta H^0 = 247 \text{ kJ mol}^{-1} \qquad (5.1)$$

The results for the MR were compared to those for the PBR to evaluate the effect of hydrogen separation in improvement in yields of the products (H_2 and CO). It is known that the reverse water-gas shift (RWGS) reaction occurs simultaneously with the reforming reaction.

$$CO_2 + H_2 \rightleftharpoons CO + H_2O \qquad \Delta H^0 = 41 \text{ kJ mol}^{-1} \qquad (5.2)$$

Therefore, the RWGS reaction was also included in the analysis. As will be seen this reaction plays an extremely important role, limiting the amount of hydrogen that can be produced at high pressures. The reforming reaction was carried out at various pressures and temperatures and, for the first time, a tradeoff in hydrogen production due to the effect of pressure on thermodynamic equilibrium and permeation rate was experimentally demonstrated.

5.2. Experimental

5.2.1. Preparation of Rh/Al_2O_3 Catalyst

A rhodium catalyst supported on Al_2O_3 was used in this work. The catalyst was prepared by the incipient wetness impregnation of γ-alumina support (Degussa, Aluminumoxid C) using an aqueous Rh solution formed from rhodium (III) chloride, $RhCl_3 \cdot 2H_2O$ (Alfa-Aesar, 99.9%). Quantities were adjusted to obtain a rhodium loading of 0.5 wt %. The impregnated support was

dried at room temperature for 24 h and calcined in air at 773 K for 6 h, and then pelletized and sieved to 30/60 mesh (0.25-0.6 mm). The number of active sites was estimated from the CO uptake at 300 K (18 μmol g^{-1}). The measurement was carried out in a volumetric chemisorption unit (Micromeritics, ASAP 2000) on 0.5 g of the sample reduced in hydrogen flow (28 μmol s^{-1}) at 873 K for 1 h. The BET surface area of the catalyst sample pretreated in identical manner was obtained from the nitrogen adsorption isotherm obtained in the same volumetric unit.

5.2.2. Preparation of Hydrogen Selective Silica Membranes

Highly hydrogen permeable and selective silica membranes were prepared by chemical vapor deposition (CVD) of a thin SiO_2 layer on a porous alumina support at either 873 K or 923 K. The reason for using the two temperatures was that the reforming reaction studies were conducted at these two temperatures. The membrane support used was a commercial multilayered porous alumina membrane (US Filter, Part No. S700-0011) of tubular geometry with 10 mm outside diameter and 1.5 mm wall thickness. The average pore size of the inside top γ-alumina layer of the membrane was 5 nm. A 5 cm length section of this porous support was connected at both ends to two pieces of the same diameter of dense alumina tubing using a high temperature glass glaze (Duncan, IN, Part No. 1001). A gas tight connection between the membrane support and the dense alumina tubing was obtained after 0.5 h of thermal treatment at 1150 K. After the connection was completed, an additional γ-Al_2O_3 layer was introduced on the inside of the support tube by dip-coating the substrate in a 0.05 M dispersion of boehmite sol for 10 s. The sample substrate was dried at room temperature for 24 h and calcined at either 873 K or 923 K for 6 h.

Deposition of the silica layer was accomplished by thermal decomposition of tetraethylorthosilicate (TEOS, Aldrich, 98%) at 873 K or 923 K in argon flow at atmospheric pressure. The alumina support substrate was installed concentrically inside a quartz glass tube of 14 mm inside diameter using machined Swagelok fittings with Teflon ferrules. After placing the assembly in an electric furnace, argon gas was introduced on both the shell side (16 μmol s^{-1}) and tube side (13 μmol s^{-1}) of the reactor, and the temperature was raised to the CVD temperature (873 K or 923 K) with a ramp of 1 K min^{-1}. The CVD process was initiated by

introducing TEOS at a concentration of 0.01 mol m^{-3} (0.024 mol %) to the inside of the porous alumina substrate. The TEOS concentration was achieved by passing argon (2.7 μmol s^{-1}) through a bubbler (at 298 K) and then mixing this flow with another stream of argon before introduction to the support tube for the CVD. The evolution of hydrogen permeance (mol m^{-2} s^{-1} Pa^{-1}) and selectivity over other gases (CH_4, CO, and CO_2) was measured as a function of silica deposition time. The silica deposition process was stopped when the hydrogen permeance of the membrane reached a value of 3×10^{-7} mol m^{-2} s^{-1} Pa^{-1}. This permeance was the same for the silica membranes used in the reforming reaction experiments. Because of a slight reduction in the permeance of the membrane with time, and also because of occasional deactivation (depending on conditions) of the catalyst employed in the studies, membranes and catalyst samples were replaced often in these studies.

5.2.3. Reforming of CH_4 with CO_2 in a Packed Bed Reactor and a Membrane Reactor

The reforming of CH_4 with CO_2 was carried out both in a hydrogen separation membrane reactor (MR) and a packed-bed reactor (PBR) of the same annular geometry. The reactions were carried out at various pressures (1, 5, 10, 15, and 20 atm) and two different temperatures (873 K and 923 K). The composition of the inlet reactant gases was fixed to CH_4:CO_2 = 1:1 for all the experiments. However, the overall inlet molar flow rate of the reactants was increased proportionally with the pressure to give the same residence time (27 s) in the reactor. The reactant inlet flow conditions are summarized in Table 5.1.

Table 5.1. Reactants inlet flow conditions

Pressure (atm)	Reactants (CH_4 + CO_2) molar flow rate (μmol s^{-1})
1	5.5
5	27.5
10	55.0
15	82.5
20	110

A schematic of the membrane reactor configuration is shown in Figure 5.1. The reactor assembly consisted of a tubular quartz glass housing with a 19 mm O.D and 2.5 mm wall thickness along with a 10 mm O.D. tubular silica membrane installed concentrically inside the quartz housing. For the case of the packed-bed reactor, the geometry was the same as the membrane reactor, but the inner tube was non-gas permeable quartz glass. A quantity of 40 mg of Rh/Al_2O_3 catalyst pellets (0.25-0.6 mm diameter) were diluted with quartz chips of the same size. The catalyst mixture was placed on the shell side of the reactor (reaction side) to make up a catalyst bed of 5 cm length (3.8 cm^3 volume) matching with the membrane zone. Inert quartz chips were also placed on the shell side of the reactor preceding the catalyst bed to provide better heat transfer and mixing of the inlet reactant gases. The reactor was assembled using machined Swagelok fittings, and the joints were sealed using an epoxy sealant (Torr-Seal, Varian) to withstand the high pressure conditions. The quartz tube proved to be durable at high pressure and temperature provided that the ends were fire-polished and the joints cooled with electric fans. Stainless steel (316) and Inconel were tried as reactor materials but were found to promote carbon formation.

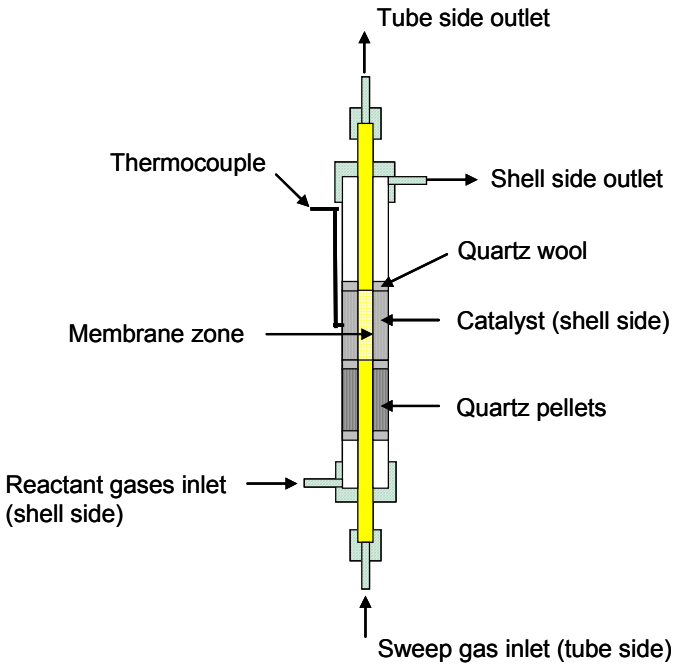

Figure 5.1. Membrane reactor configuration

A schematic of the reactor system is shown in Figure 5.2. The reactor assembly was installed in an electrical furnace, and the temperature was raised to the reaction temperature with argon flowing through the shell side (21 μmol s^{-1}) and tube side (27 μmol s^{-1}) of the reactor. After the temperature reached the reaction temperature (873 K or 923 K) the shell side argon flow was stopped and hydrogen flow (21 μmol s^{-1}) was introduced for 1 h to reduce the catalyst. After the catalyst reduction the reforming reaction was initiated by introducing the reactant gases (CH_4 and CO_2) to the shell side of the reactor. The pressure on the shell side of the reactor (reaction side) was adjusted using a back-pressure regulator. On the tube side (permeate side), argon flow (27 μmol s^{-1}) was kept as a sweep gas at atmospheric pressure. The outlet stream from the shell side passed through an ice bath to remove moisture from the stream. The flow rate of the outlet stream from the shell side of the reactor was measured using a bubble flow meter. This stream was then injected into a gas chromatograph (GC, SRI 8610B) equipped with a thermal conductivity detector to measure the concentration of CH_4, CO_2, CO, and H_2. The molar flow rate of the species was calculated using the measured concentration and the overall outlet volumetric flow rate. For the case of water, the flow rate was obtained as the average of the calculated values from hydrogen and oxygen balances. The same procedure was applied separately to the tube side of the reactor. The conversion and utilization of the reactants (CH_4 and CO_2) were calculated with the following equations using the molar flow rates of each species from the inlet and outlet of the reactor:

$$Conversion(i) = \frac{(F_i^{in} - F_i^{out})}{F_i^{in}} \tag{5.3}$$

$$Utilization(i) = F_i^{in} - F_i^{out} \tag{5.4}$$

where F_i^{in} is the inlet flow rate (mol s^{-1}) of reactant species i, and F_i^{out} is the outlet flow rate (mol s^{-1}) of residual reactant species i measured at the end of the reactor. For the MR the conversion and utilization were calculated using the sum of flow rates of individual reactant species in the shell side and tube side.

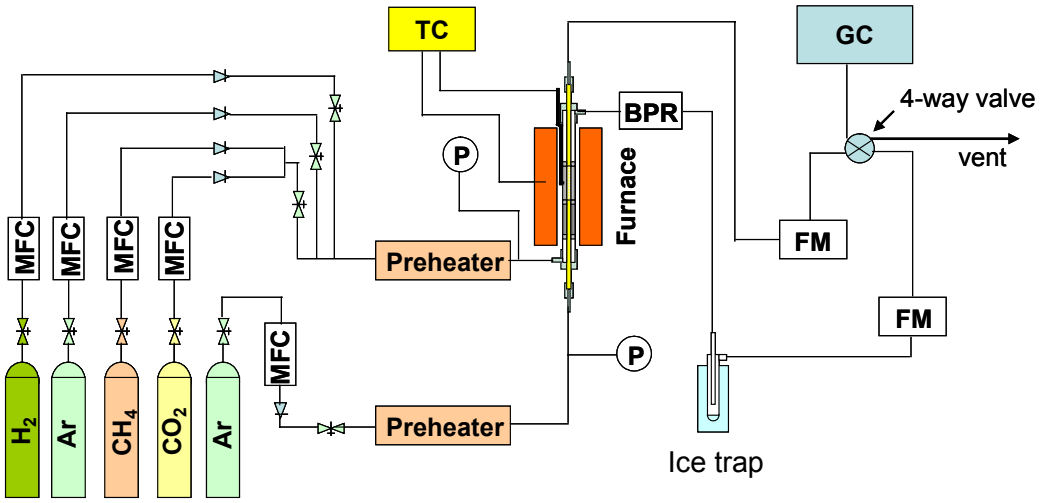

Figure 5.2. A schematic of the reactor system

MFC: Mass Flow Controller	TC: Temperature Controller
P: Pressure Gauge	BPR: Back Pressure Regulator
FM: Flow Meter	GC: Gas Chromatograph

5.3. Results

5.3.1. Properties of the Catalyst and Membranes

The BET surface area and the CO uptake of the Rh/Al_2O_3 catalyst are shown in Table 5.2. The dispersion of rhodium on the support calculated from the above data was 40 %.

Table 5.2. BET surface area and CO uptake of the Rh/Al_2O_3 catalyst (0.5 % of Rh loading)

BET surface area (m^2g^{-1})	CO uptake ($\mu mol\ g^{-1}$)
93	18

The permeances (mol m^{-2} s^{-1} Pa^{-1}) of H_2, CH_4, CO, and CO_2 through the silica membranes are shown versus silica deposition time at 873 K and 923 K in Figure 5.3. Initially, the fresh alumina supports had very high permeance for all the gases ([873 K] H_2: 2.2×10^{-5}, CH_4: 9.7×10^{-6}, CO: 7.1×10^{-6}, CO_2: 5.4×10^{-6} mol m^{-2} s^{-1} Pa^{-1}; [923 K] H_2: 2.1×10^{-5}, CH_4: 9.4×10^{-6}, CO: 6.9×10^{-6}, CO_2: 5.2×10^{-6} mol m^{-2} s^{-1} Pa^{-1}). During the progress of the silica deposition, the permeance of hydrogen showed a moderate decrease while the permeance of the other gases showed a significant decrease at both the temperatures. A hydrogen permeance of 3×10^{-7} mol m^{-2} s^{-1} Pa^{-1} was reached after 4.5 h of silica deposition at 873 K, while the same hydrogen permeance was obtained after only 1.7 h of silica deposition at 923 K. After the silica layer deposition the permeance of the other gases decreased significantly ([873 K] CH_4: 1.0×10^{-9}, CO: 1.4×10^{-9}, CO_2: 1.8×10^{-9} mol m^{-2} s^{-1} Pa^{-1}; [923 K] CH_4: 1.2×10^{-9}, CO: 1.5×10^{-9}, CO_2: 1.8×10^{-9} mol m^{-2} s^{-1} Pa^{-1}) showing a four order of magnitude drop from their initial values on the fresh alumina support. Before silica deposition the permeance order of the gases on the fresh alumina support was $H_2 > CH_4 > CO > CO_2$. However, the permeance order changed after silica deposition to $H_2 > CO_2 > CO > CH_4$.

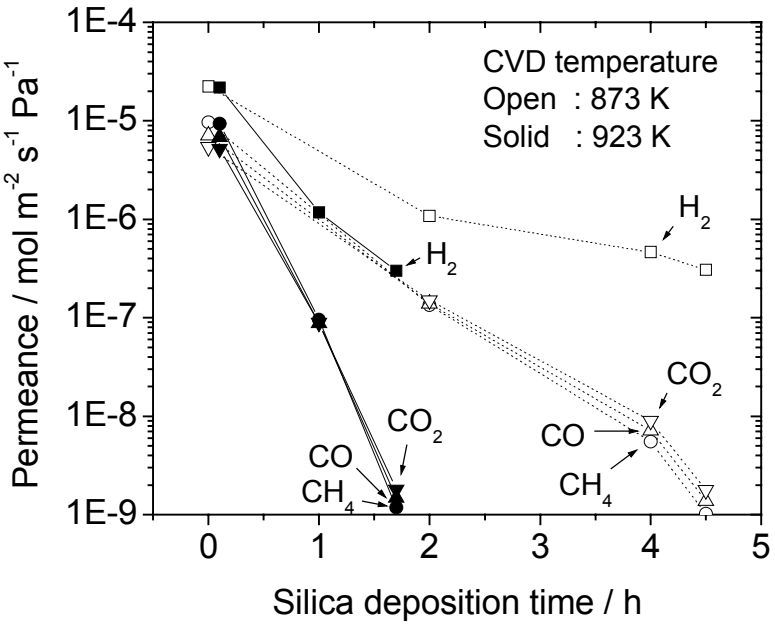

Figure 5.3. Permeance vs. silica deposition time

Figure 5.4 shows the selectivities for hydrogen over other gases for the silica membranes as a function of the hydrogen permeance at the CVD temperature of 873 K and 923 K. Before silica deposition the fresh alumina supports had low selectivities of hydrogen over other gases at both the temperatures ([873 K] CH_4: 2.32, CO: 3.15, CO_2: 4.13; [923 K] CH_4: 2.32, CO: 3.17, CO_2: 4.14). During the early stage of silica deposition, the selectivities for hydrogen increased only moderately while the hydrogen permeance decreased relatively rapidly at both temperatures. At later stages the hydrogen selectivity increased significantly while the hydrogen permeance decreased only slightly. At a hydrogen permeance of 3×10^{-7} mol m^{-2} s^{-1} Pa^{-1}, the selectivities of hydrogen over other gases reached values exceeding 200 at both temperatures used in this study ([873 K] CH_4: 300, CO: 220, CO_2: 170; [923K] CH_4: 250, CO: 200, CO_2: 170).

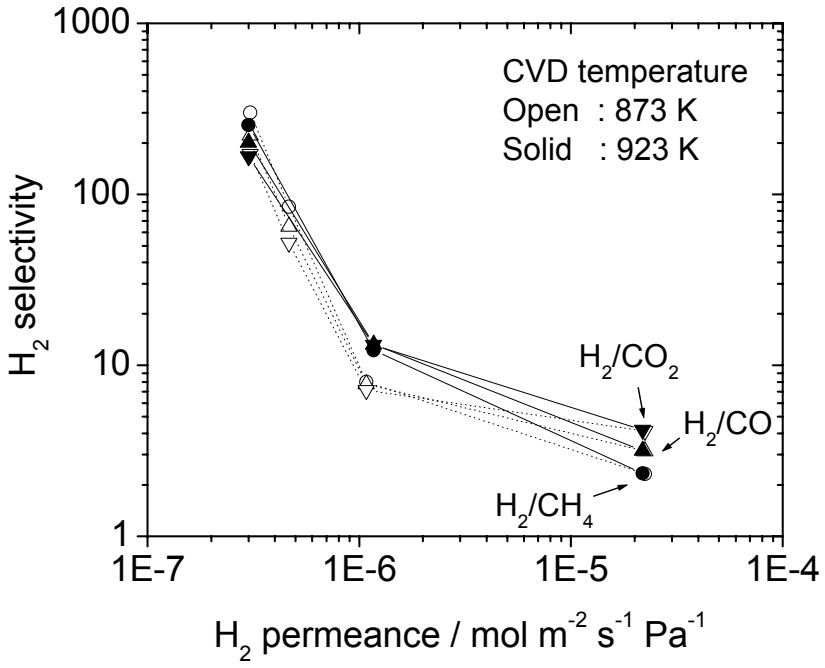

Figure 5.4. Hydrogen selectivity vs. H_2 permeance

5.3.2. The CH_4/CO_2 Reforming in the Packed Bed and Membrane Reactor

5.3.2.1. Conversions of the reactants (CH_4 and CO_2)

The experimental conversions (solid lines) of methane and carbon dioxide in the packed-bed reactor (PBR) and the membrane reactor (MR) were obtained as a function of pressure at 873 K (Fig. 5.5a) and 923 K (Fig. 5.5b). The theoretical equilibrium conversions of CH_4 and CO_2 were calculated by solving simultaneously the following equations for the dry reforming reaction (Eq.5.1) and the reverse water-gas shift reaction (Eq. 5.2):

$$K_2 = \frac{y_{CO}^2 y_{H_2}^2}{y_{CH_4} y_{CO_2}} P^2 \tag{5.5}$$

$$K_3 = \frac{y_{CO} y_{H_2O}}{y_{CO_2} y_{H_2}} \tag{5.6}$$

where K_2 (873 K = 0.19, 923 K = 1.31) is the equilibrium constant for the dry reforming reaction, K_3 (873 K = 0.37, 923 K = 0.48) is the equilibrium constant for the reverse water-gas shift reaction (RWGS), y_i is the mole fraction of species i, and P is the pressure (atm). The theoretical equilibrium conversion results (dotted lines) are also displayed in Figures 5.5a) and 5.5b). The calculations show that the equilibrium conversion of CH_4 and CO_2 decrease with increasing pressure and increase with increasing temperature. The calculations also show that the equilibrium conversion of CO_2 is higher than that of CH_4 at all conditions.

In the PBR, it was found that the experimental CH_4 and CO_2 conversions were below equilibrium for all the pressures and temperatures in this work. At both 873 K and 923 K, the experimental conversions of CO_2 in the PBR were higher than those of CH_4. The conversion of CO_2 and CH_4 in the PBR decreased with increasing pressure. As can be seen in Figures 5.5a) and 5.5b), the decrease of the conversions was steep at low pressures but rather moderate at higher pressures. An increase in the reaction temperature from 873 K to 923 K resulted in higher conversions for both CO_2 and CH_4 at all the pressures.

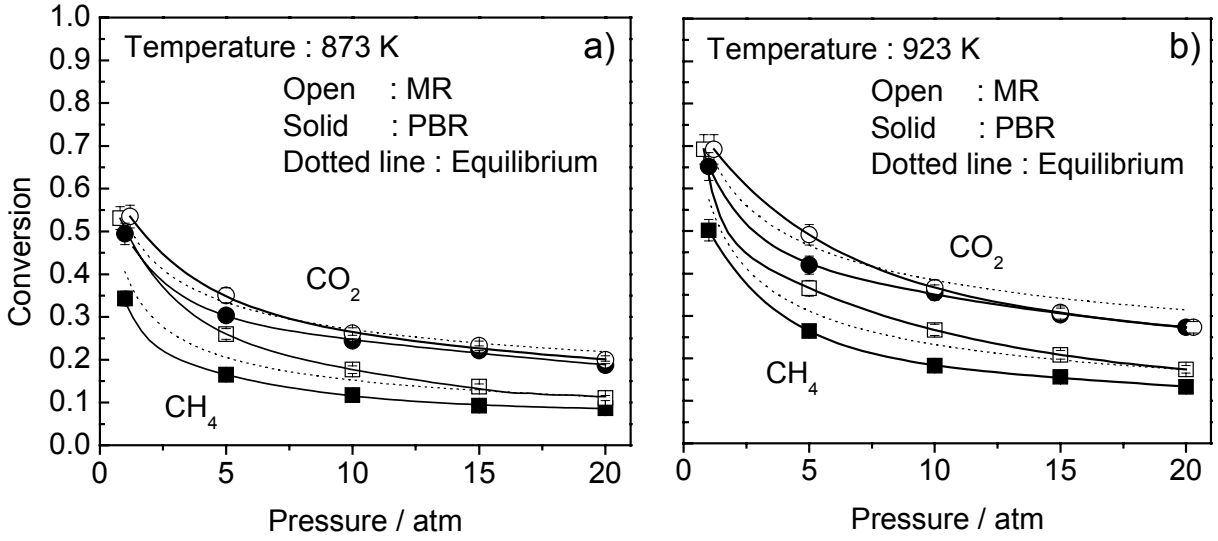

Figure 5.5. Conversions vs. reaction pressure

In the MR, the experimental conversions of both CH_4 and CO_2 in the MR were higher than the conversion obtained in the PBR for all the pressures and temperatures in this work. The conversions of CO_2 and CH_4 in the MR even exceeded the equilibrium conversions especially in the low pressure range. For example at 873 K (Fig. 5.5a)) and 1 atm, the fractional conversions of CO_2 and CH_4 in the MR (CO_2: 0.54, CH_4: 0.53) were above the equilibrium conversions (CO_2: 0.53, CH_4: 0.41) and were considerably higher than the conversions obtained in the PBR at the same pressure (CO_2: 0.50, CH_4: 0.34). Also of interest, while the conversions of CO_2 and CH_4 were significantly different in the PBR ($CO_2 > CH_4$), the conversions found in the MR were closer. As the reaction pressure increased, the conversions of CO_2 and CH_4 in the MR decreased and approached the conversion values of CO_2 and CH_4 in the PBR. At 20 atm, the conversions of CO_2 and CH_4 in the MR (CO_2: 0.20, CH_4: 0.11) were slightly higher than the conversions obtained in the PBR (CO2: 0.19, CH4: 0.09).

An increase of the reaction temperature from 873 K to 923 K resulted in higher conversions for both CH_4 and CO_2 at all pressures. At 923 K (Fig. 5.5b) and 1 atm, the conversions of CO_2 and CH_4 in the MR (CO_2: 0.69, CH_4: 0.69) were also above equilibrium and higher than the conversions obtained in the PBR at the same pressure (CO_2: 0.65, CH_4: 0.50). Again, the conversions of CO_2 and CH_4 in the MR at these conditions were comparable while the conversions found in the PBR were significantly different. Similar to the behavior at 873 K, the conversions of CO_2 and CH_4 in the MR decreased with increasing pressure and approached those values found in the PBR at high pressures. This trend was particularly rapid for CO_2. The conversions of CO_2 and CH_4 in the MR at 923 K and 20 atm (CO_2: 0.27, CH_4: 0.17) were only slightly higher than those in the PBR at the same conditions (CO_2: 0.26, CH_4: 0.13).

5.3.2.2. Utilization of CH_4 and CO_2

The experimental utilizations (mol s^{-1}) of CH_4 and CO_2 in the PBR and in the MR are shown (solid lines) versus pressure at 873 K in Figure 5.6a). The results for 923 K are shown in Figure 5.6b). The equilibrium utilizations of CH_4 and CO_2 were calculated using the equilibrium conversion data and the inlet flow rates of the reactants (Table 5.1). The results (dotted lines) are also displayed in Figures 5.6a) and 5.6b).

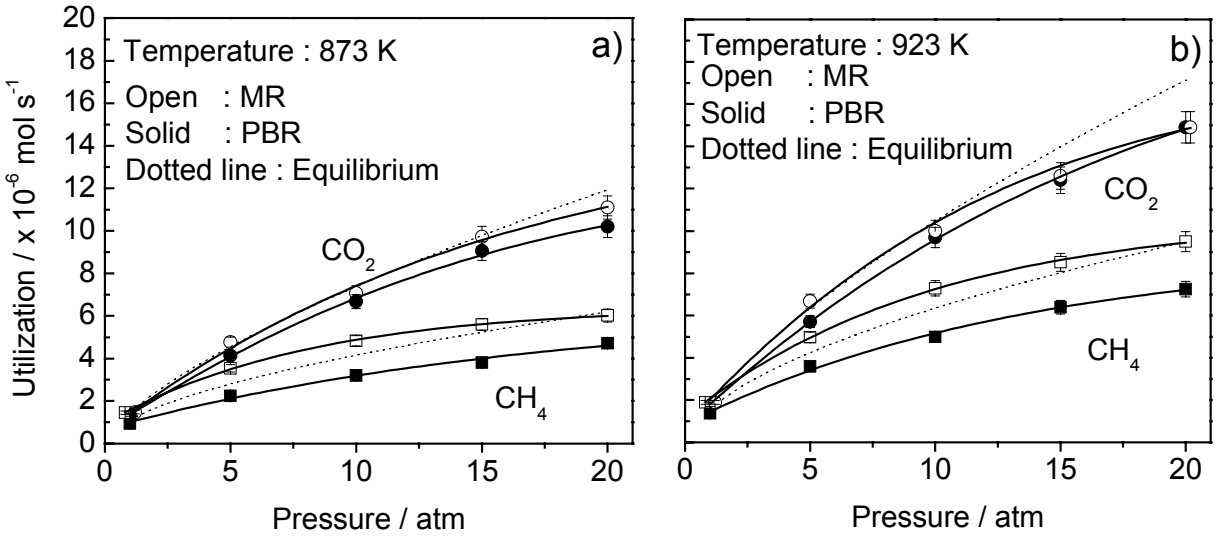

Figure 5.6. Reactant utilization vs. reaction pressure

In the PBR, the experimental utilizations of CH_4 and CO_2 were below the equilibrium utilizations at all the pressures and temperatures in this work. At both 873 K and 923 K, the utilizations of CH_4 and CO_2 in the PBR showed a considerable increase with increasing pressure. However, the increase in the utilization was not linear with pressure, levelling-off at high pressures. The increase was more significant for CO_2 than for CH_4, resulting in a clear utilization order of $CO_2 > CH_4$ at high pressures. The utilizations of CO_2 and CH_4 were close to equilibrium at atmospheric pressure, but showed an increasing deviation from the equilibrium utilizations at higher pressures. An increase of reaction temperature from 873 K to 923 K resulted in higher utilizations for both CO_2 and CH_4 at all pressures.

In the MR, enhancements in the utilizations of both CH_4 and CO_2 over the PBR were observed for all the pressures and temperatures used in this work. For example at 873 K (Fig. 5.6a)) and 1 atm, the utilizations of CO_2 and CH_4 in the MR (CO_2: 1.46×10^{-6}, CH_4: 1.45×10^{-6} mol s^{-1}) were higher than the utilizations obtained in the PBR at the same pressure (CO_2: 1.35×10^{-6}, CH_4: 9.36×10^{-7} mol s^{-1}). The enhancement was particularly noticeable for CH_4, resulting in a utilization above equilibrium. The utilizations of both CH_4 and CO_2 in the MR increased with increasing pressure. At 20 atm, the utilizations of both CO_2 and CH_4 in the MR (CO_2: 1.11×10^{-5}, CH_4: 6.02×10^{-6} mol s^{-1}) were significantly higher than the utilizations achieved at 1 atm

in the MR. The utilization of both CO_2 and CH_4 in the MR were also higher at 20 atm than the utilizations obtained in the PBR (CO_2: 1.02×10^{-5}, CH_4: 4.72×10^{-6} mol s^{-1}).

An increase of temperature from 873 K to 923 K resulted in higher utilizations for both CH_4 and CO_2. At 923 K (Fig. 5.6b)) and 1 atm, the utilizations of CO_2 and CH_4 in the MR (CO_2: 1.89×10^{-6}, CH_4: 1.89×10^{-6} mol s^{-1}) were also comparable to each other, and higher than those in the PBR (CO_2: 1.78×10^{-6}, CH_4: 1.37×10^{-6} mol s^{-1}). The utilization of CH_4 in the MR increased with pressure, maintaining higher values than those in the PBR and higher than equilibrium except at the highest pressure. The utilization of CO_2 in the MR also increased with increasing pressure, but at 923 K showed an approach to the utilization obtained in the PBR at high pressures. At 20 atm, the utilizations of CO_2 and CH_4 in the MR (CO_2: 1.50×10^{-5}, CH_4: 9.50×10^{-6} mol s^{-1}) were also higher than those in the PBR (CO_2: 1.49×10^{-5}, CH_4: 7.25×10^{-6} mol s^{-1}). However, the enhancement was small in the case of CO_2.

5.3.2.3. Yields of the reaction products (H_2, CO, and H_2O)

Yields are defined in this study as the molar rates of formation of the products of the reaction.

$$Yield(j) = F_j^{out} \tag{5.7}$$

where F_j^{out} is the reactor outlet molar flow rate (mol s^{-1}) of product j. For the MR the yields are the sum of the tube side and shell side products. The yields of the reaction products (CO, H_2 and H_2O) in the PBR and in the MR are shown (solid lines) versus various pressures at 873 K in Figure 5.7a). The results for 923 K are shown in Figure 5.7b). The equilibrium yields of the products were calculated and also displayed (dotted lines) in Figures 5.7a) and 5.7b).

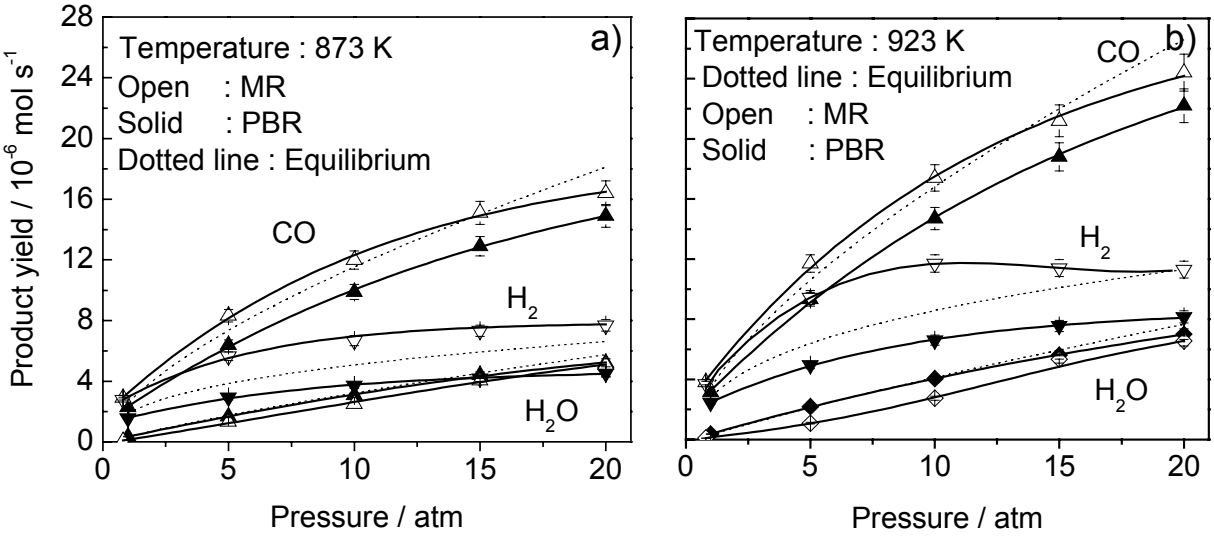

Figure 5.7. Yields of the reaction products vs. reaction pressure

In the PBR, the experimental yields of CO, H_2 and H_2O were below equilibrium at all the pressures and temperatures. At both 873 K and 923 K, the yields of CO, H_2 and H_2O in the PBR increased with increasing pressure but the pressure dependence was different for each product. Basically, the yields of CO and H_2O showed a continuous and rapid increase with increasing pressure while the yield of H_2 displayed a limited increase and reached a plateau at high pressures. For example, at 873 K (Fig. 5.7a)) and 1 atm, the yields of the products in the PBR were low, and showed an order in yield of CO > H_2 > H_2O. It should be noted that the increase in yields with increasing pressure were significantly higher for CO and H_2O than that for H_2, which resulted in an order in yield of CO > H_2O > H_2 at 20 atm. An increase of temperature from 873 K to 923 K resulted in higher yields of CO, H_2 and H_2O at all pressures, but the pressure dependence of the yields of the products was similar to that observed at 873 K. At 923 K (Fig. 5.7b)), the yields of CO and H_2O also increased considerably with increasing pressure, but the yield of H_2 again showed a limited rise with increasing pressure. The yields of the products followed the order of CO > H_2 > H_2O at all pressures. However, the yield of H_2O became comparable to the yield of H_2 at high pressures.

The yields of the products in the MR were different from those in the PBR. At both 873 K and 923 K, enhancements in the yields of CO and H_2 were observed in the MR at all pressures. Conversely, the yields of H_2O in the MR were lower than those obtained in the PBR. For example at 873 K (Fig. 5.7a)) and 1 atm, the yields of CO and H_2 in the MR (CO: 2.91×10^{-6}, H_2: 2.77×10^{-6} mol s^{-1}) were higher than those in the PBR (CO: 2.29×10^{-6} H_2: 1.56×10^{-6} mol s-1), while the yield of H_2O in the MR (7.00×10^{-8} mol s^{-1}) was lower than that in the PBR (3.61×10^{-7} mol s^{-1}). The yields of all the products in the MR increased with increasing pressure. At 873 K and 20 atm, the yields of CO and H_2 in the MR (CO: 1.64×10^{-5}, H_2: 7.68×10^{-6} mol s^{-1}) were significantly higher than the yields obtained in the PBR (CO: 1.49×10^{-5}, H_2: 4.53×10^{-6} mol s^{-1}) whereas the yield of H_2O in the MR (5.08×10^{-6} mol s^{-1}) remained lower than the yield obtained in the PBR (5.21×10^{-6} mol s^{-1}). An increase of reaction temperature from 873 K to 923 K gave rise to higher yields for CO, H_2, and H_2O at all pressures. At 923 K (Fig 5.7b)) and 1 atm, the yields of CO and H_2 in the MR (CO: 3.81×10^{-6}, H_2: 3.69×10^{-6} mol s^{-1}) were again higher than the yields obtained in the PBR (CO: 3.15×10^{-6}, H_2: 2.45×10^{-6} mol s^{-1}). Conversely, the yield of H_2O in the MR (9.00×10^{-8} mol s^{-1}) was lower than the yield in the PBR (3.50×10^{-7} mol s^{-1}). The yield of CO and H_2O in the MR increased rather gradually with increasing pressure whereas the yields of H_2 in the MR showed a plateau as pressure was raised. This was particularly evident at 923 K, where a maximum occurred. At 923 K and 20 atm, the yield of CO and H_2 in the MR (CO: 2.44×10^{-5}, H_2: 1.13×10^{-5} mol s^{-1}) was again higher than the yields in the PBR (CO: 2.22×10^{-5}, H_2: 8.15×10^{-6} mol s^{-1}), while the yield of H_2O in the MR (6.55×10^{-6} mol s^{-1}) was slightly lower than the yield in the PBR (6.98×10^{-6} mol s^{-1}).

5.4. Discussion

The silica membrane used in this study was highly hydrogen permeable and moderately selective over other gases. Details on the characterization and gas permeation mechanism of the membrane were reported in preceding chapters. Briefly, the methodology used in the membrane preparation consisted of placing a thin hydrogen selective silica layer (10-20 nm) on top of a porous alumina support to provide high hydrogen selectivities while maintaining a high hydrogen permeance. The porous alumina support had high permeance for hydrogen but low

selectivities of hydrogen over other gases. This was because the mechanism of gas transport in the porous alumina membrane support was mainly by Knudsen diffusion, in which the rate of gas transport was proportional to the inverse square root of temperature and molecular weight of the gases. The permeance of gases on the porous alumina support showed an order of $H_2 > CH_4 > CO > CO_2$ consistent with the inverse molecular weight dependence expected from the Knudsen diffusion mechanism. The selectivities of hydrogen over other gases on the porous support ([873 K] CH_4: 2.3, CO: 3.2, CO_2: 4.1; [923 K] CH_4: 2.3, CO: 3.2, CO_2: 4.1) showed agreement to Knudsen selectivity values (CH_4: 2.8, CO: 3.7, CO_2: 4. 7). After silica deposition, the selectivity of hydrogen over other gases increased significantly exceeding values above 200, while the permeance of hydrogen (3×10^{-7} mol m^{-2} s^{-1} Pa^{-1}) remained high. Note that after silica deposition the permeance order changed to $H_2 > CO_2 > CO > CH_4$, which was in the order of increasing molecular size of gases (H_2 = 0.289 nm, CO_2 = 0.33 nm, CO = 0.376 nm, CH_4 = 0.38 nm [i]). This indicates that the origin of the high hydrogen selectivity on the silica membrane was size differentiation provided by small solubility sites in the thin silica layer placed on the alumina support.

The results shown in Figures 5.5a) and 5.5b) indicated that the conversions in the CH_4/CO_2 reforming reaction system increased at high temperature and decreased at high pressure, consistent with the expectations from thermodynamics for this endothermic reaction with an increase in moles. In the PBR, the conversion of both CH_4 and CO_2 were below equilibrium due to the small amount of catalyst used (40 mg, 0.7 μmol CO uptake) compared to the flow of reactants (5 μmol s^{-1} at 1 atm, Table 5.1) used in the experiments. The reaction experiments using different catalyst loading and pellet size indicated that the non-equilibrium conversions obtained in the above results were not due to heat or mass transport limitation. Nevertheless, the experimental CH_4 and CO_2 conversions in the PBR followed the trend that was expected from equilibrium. The experimental conversion of CO_2 was higher than the conversion of CH_4 at all conditions due to the occurrence of the RWGS reaction in which CO_2 reacted with the H_2 produced from the reforming reaction. The contribution of the concurrent separation of hydrogen from the reactions was clear in the MR which showed higher conversions of both CH_4 and CO_2 than the PBR.

The effects of pressure and temperature on the rates of the reactions (dry reforming and RWGS) do not explicitly appear in the conversion results, because the conversions represent fractions of reactants transformed. For this reason productivity results were described as utilization of reactants ($Utilization(i)\,[mol\ s^{-1}] = F_i^{in} - F_i^{out}$) and yield of products ($Yield(j)\,[mol\ s^{-1}] = F_j^{out}$), which directly describe the amounts of species consumed or formed. For the PBR, the results (Fig 5.6a) and 5.6b)) showed that the experimental CH_4 and CO_2 utilizations increased with increasing reaction pressure indicating that the rates of the reactions were enhanced at high pressures. Note that to keep the nominal contact time constant with pressure, the volumetric flow rate of the reactants in the reactor was kept the same by varying the inlet molar flow rate of the reactants. Note also that the conversions of CH_4 and CO_2 in the PBR were below equilibrium at all conditions. Therefore, the increase in the utilization of CH_4 and CO_2 at high pressures was not due to an increase in residence time of the reactants in the reactor. In fact, the rate of increase in both CH_4 and CO_2 utilizations became smaller at higher pressures indicating that the effect of pressure on the rates of the reactions decreased as the pressure increased. This is because of the increase in the contribution of the backward reaction in dry reforming, as will become evident in the discussion of equilibrium quotients results later on.

For the MR, Figures 5.6a) and 5.6b) clearly show the enhancements in the utilization of CH_4 and CO_2 over the PBR. At both 873 K and 923 K, the utilizations of CH_4 and CO_2 in the MR were higher than those obtained in the PBR. The enhancements were significantly higher for CH_4 than for CO_2 at all the pressures. The results can be described using a utilization ratio of the reactants (CO_2/CH_4), and this is displayed at various reaction pressures for the MR and the PBR at 873 K (Fig. 5.8a)) and 923 K (Fig. 5.8b)). The utilization ratio of CO_2 and CH_4 is a measure of the contribution of the RWGS reaction in the overall reaction system. The results show that the utilization ratio in the MR was always lower than in the PBR at all the pressures and temperatures. This was because the simultaneous separation of hydrogen through the membrane in the MR suppressed the occurrence of RWGS reaction, in which H_2 is the co-reactant with CO_2 for the reaction. The results also show that the utilization ratio increased with pressure both in the PBR and MR. This indicates that increasing pressure gave rise to an enhanced contribution of RWGS reaction in the reaction. However, the utilization ratio in the MR remained lower than that in the PBR at all the pressures.

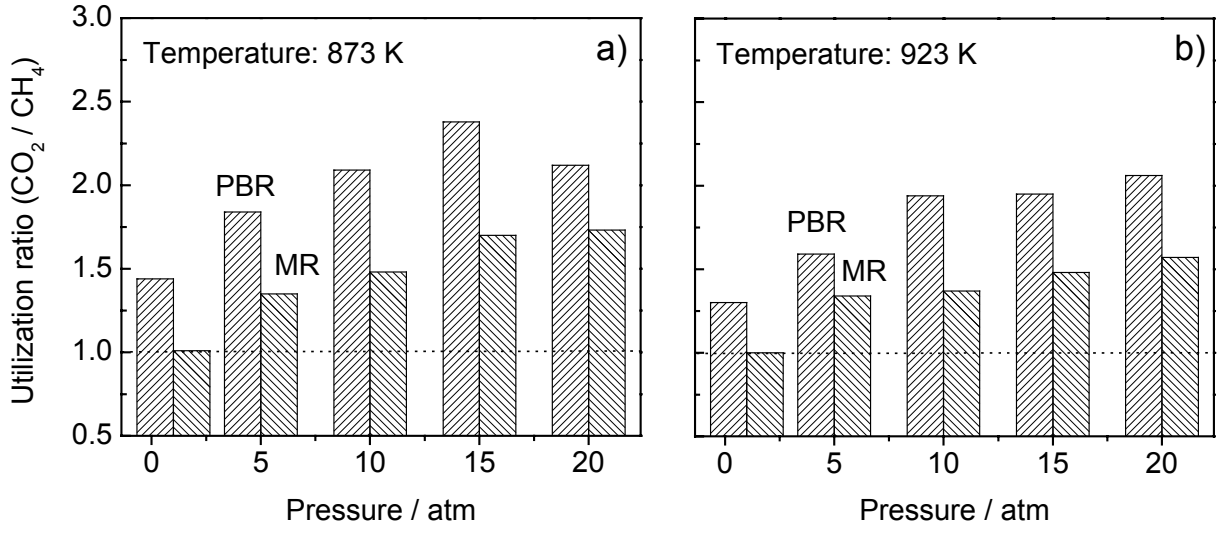

5.8. Utilization ratio of the reactants (CO_2/CH_4) vs. reaction pressure

Figures 5.7a) and 5.7b) show that the yields of the reaction products (CO, H_2, and H_2O) in the PBR increased with reaction pressure. The increase was more significant for CO and H_2O than for H_2. The yields of CO and H_2O in the PBR showed a gradual increase with pressure while the yield of H_2 was significantly reduced, reaching a plateau at high pressures. At 20 atm the yield of H_2 was less than half that of CO in both the MR and PBR. The results are consistent with the findings discussed in the previous section, namely that an increase in pressure resulted in an enhanced contribution of the RWGS reaction to the system. As a consequence, hydrogen produced from the dry reforming reaction was consumed at high pressures producing H_2O and additional CO. The occurrence of the RWGS reaction resulted in higher yields of CO than of H_2 at all conditions. The ratio of CO and H_2 yields (CO/H_2) in the PBR and in the MR is shown versus pressure in Figures 5.9a) and 5.9b). The results showed that the CO/H_2 yield ratio in the PBR increased significantly with reaction pressure, indicating an increasing contribution of the RWGS reaction to the system. An increase in temperature from 873 K to 923 K resulted in lower CO/H_2 yield ratios for all pressures. The CO/H_2 yield ratio in the MR was below the ratio obtained in the PBR indicating that the continuous separation of hydrogen from the reaction system resulted in a reduced contribution of the RWGS reaction. This was also indicated in Figures 5.7a) and 5.7b) where the yields of H_2O in the MR were lower than the yields in the PBR.

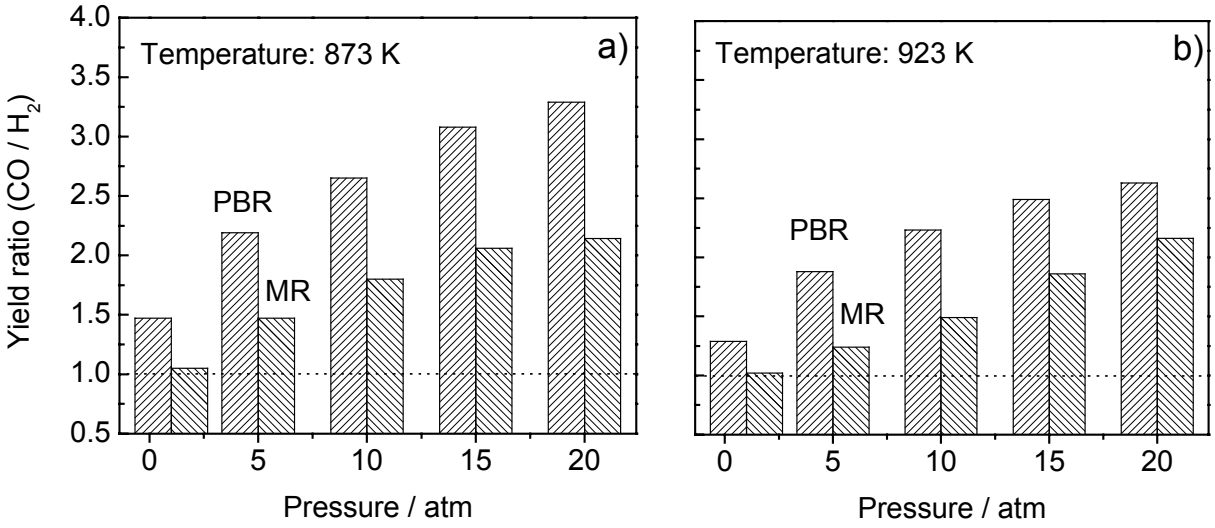

Figure 5.9. Yield ratio (CO/H_2) vs. reaction pressure

The results obtained here on product yields are important. The dry-reforming reaction has been often cited as an attractive alternative to steam-reforming for syngas production because of its usage of CO_2. Until now most studies were carried out at atmospheric pressure where the products consisted of almost equimolar amounts of H_2 and CO, and the problem was not recognized. However, our studies at high pressure clearly show that the dry-reforming reaction is impractical because of the consumption of H_2 by the RWGS reaction. This diverts H_2 to H_2O. The problem is general, regardless of the catalyst employed or the use of a membrane reactor, because of the higher reactivity of H_2 than CH_4 for CO_2.

The influence of hydrogen separation on both the dry reforming reaction and the RWGS reaction may be analyzed in a quantitative way by comparing experimental K_2 (dry reforming, Eq 5.5) and K_3 (RWGS, 5.6) quotients to the equilibrium constant values of the respective reactions. The term quotient is used here to distinguish between experimentally determined quantities and true equilibrium constants obtained from thermodynamic data. The experimental K_2 and K_3 quotients in the PBR and in the MR were calculated using equations (5.5) and (5.6) but utilizing the species compositions at the outlet of the reactors. In the case of the MR, the

experimental values obtained were for the shell side (reaction side) of the reactor. The results are summarized along with theoretical equilibrium values in Table 5.3.

Table 5.3. Experimental K_2 and K_3 quotients for the dry reforming reaction and the RWGS reaction.

Temp (K)	Pressure (atm)	$CH_4 + CO_2$ F $2\,CO + 2\,H_2$ Dry reforming reaction (K_2)		$CO_2 + H_2$ F $H_2O + CO$ RWGS reaction (K_3)	
		PBR	MR	PBR	MR
873		Equilibrium $K_2 = 0.19$		Equilibrium $K_3 = 0.37$	
	1	0.09	0.10	0.38	0.19
	5	0.08	0.05	0.39	0.79
	10	0.07	0.05	0.39	0.64
	15	0.07	0.04	0.42	0.78
	20	0.06	0.03	0.39	0.65
923		Equilibrium $K_2 = 1.31$		Equilibrium $K_3 = 0.48$	
	1	0.68	0.72	0.48	0.32
	5	0.57	0.41	0.52	0.70
	10	0.56	0.40	0.51	0.69
	15	0.51	0.39	0.49	0.73
	20	0.45	0.39	0.48	0.61

The results showed that the experimental K_3 quotients for the RWGS reaction in the PBR were close to the equilibrium K_3 value at all the pressures and temperatures. The small deviations are due to experimental error. This indicated that the RWGS reaction was in equilibrium in the PBR at all the conditions in this work. However, the experimental K_2 quotients in the PBR were considerably lower than the equilibrium K_2 value. It could be deduced from the results that the rate of the RWGS reaction was much faster than the rate of the dry reforming reaction at the pressure and temperature conditions used in this work. In fact, the higher rate for the RWGS reaction compared to the dry reforming reaction has been reported in the literature [ii,iii]. This makes sense, and is expected to be general, as the RWGS involves the reaction of H_2 with CO_2 while the dry reforming that of CH_4 and CO_2, and H_2 is more reactive than CH_4 on most catalysts.

The experimental K_2 and K_3 quotients in the MR were different from those in the PBR. Except at 1 atm, the experimental K_3 quotients for the RWGS reaction in the MR were higher than the equilibrium K_3 value. This indicated that the separation of hydrogen at high pressures from the MR was significant and fast. In contrast, the experimental K_2 quotients for the dry reforming reaction in the MR were less than the equilibrium K_2 value and also lower than the K_2 quotient obtained in the PBR (except at 1 atm where the K_2 values in the MR and PBR were comparable). These results indicated that the separation of hydrogen from the reaction system in the MR provided an enhanced thermodynamic driving force to the dry reforming reaction. As the pressure increased deviation in the experimental K_2 quotient from equilibrium values were observed for both reactors. This was due to the enhancement of the reverse reaction over the forward reaction as pressure increased and can be understood from the higher reactivity of the CO and H_2 products than the CH_4 and CO_2 reactants. As pressure increased not only did the equilibrium conversions go down but the reactions were driven further and further away from equilibrium. The values of the K_2 quotients demonstrate that the dry-reforming reaction operates in a non-equilibrium regime in both the PBR and MR. The removal of H_2 in the membrane reactor causes the K_2 quotient in the MR to deviate even more than in the PBR. The enhancements in yields of products shown in Fig. 5.7 demonstrate that membrane reactors give superior performance over PBR even under non-equilibrium conditions.

In order to evaluate the magnitude of the hydrogen separation in the MR, the percentage H_2 separation was calculated using the following equation,

$$H_2 separation = \frac{F_{H_2}(tube)}{F_{H_2}(tube) + F_{H_2}(shell)} \times 100 \qquad (5.8)$$

where F_{H_2} is the molar flow rate of hydrogen either on the shell side or the tube side of the reactor. The calculation results are shown versus various pressures at 873 K (Fig. 5.10a) and 923 K (Fig. 5.10b) with 95% confidence limits displayed. The results indicated that the amount of hydrogen separated through the membrane from the reaction side (shell side) of the MR was significant for all the pressures and temperatures used in this work. For example at 873 K, the separated hydrogen accounted for more than 60 % of the total hydrogen yield in the MR at all the pressures. The separation of hydrogen initially increased in the low pressure range reaching a maximum separation of about 70 % at 5 atm. The separation of hydrogen then decreased at the higher pressures. Similar behavior was observed at 923 K. The hydrogen separation increased

with increasing pressure showing a clear maximum at 5 atm, then decreased steadily at higher pressures. The initial increase is due to the higher permeability of H_2 at higher pressure, while the decline is due to the lower availability of H_2 due to equilibrium.

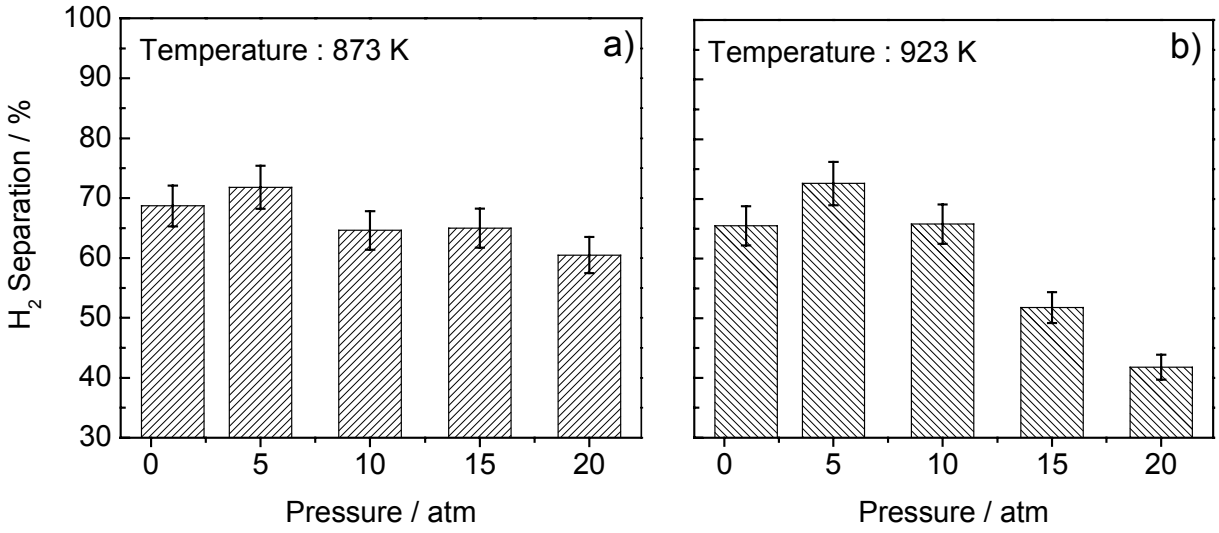

Figure 5.10. Hydrogen separation vs. reaction pressure

The yields of hydrogen in the MR were compared to the yields in the PBR in order to evaluate the enhancements in the hydrogen yields. The enhancement is defined as $Y_j(MR) / Y_j(PBR) \cdot 100$. The results are shown versus pressure in Figures 5.11a) and 5.11b), again with 95% confidence intervals marked. It is apparent that there were significant increases in hydrogen yields in the MR. For example at 873 K, the hydrogen yields in the MR showed over 170 % enhancement over those in the PBR at all pressures. The enhancement increased with increasing pressure reaching a maximum at 5 atm, where the yield of hydrogen in the MR was about twice that in the PBR. The enhancements of the hydrogen yields then decreased at higher pressures. The same behavior was observed at 923 K, showing a clear pressure dependency. The enhancements at 923 K were above 140 % for all the pressures and a maximum enhancement was achieved at 5 atm, where the yield in the MR was again about twice that in the PBR.

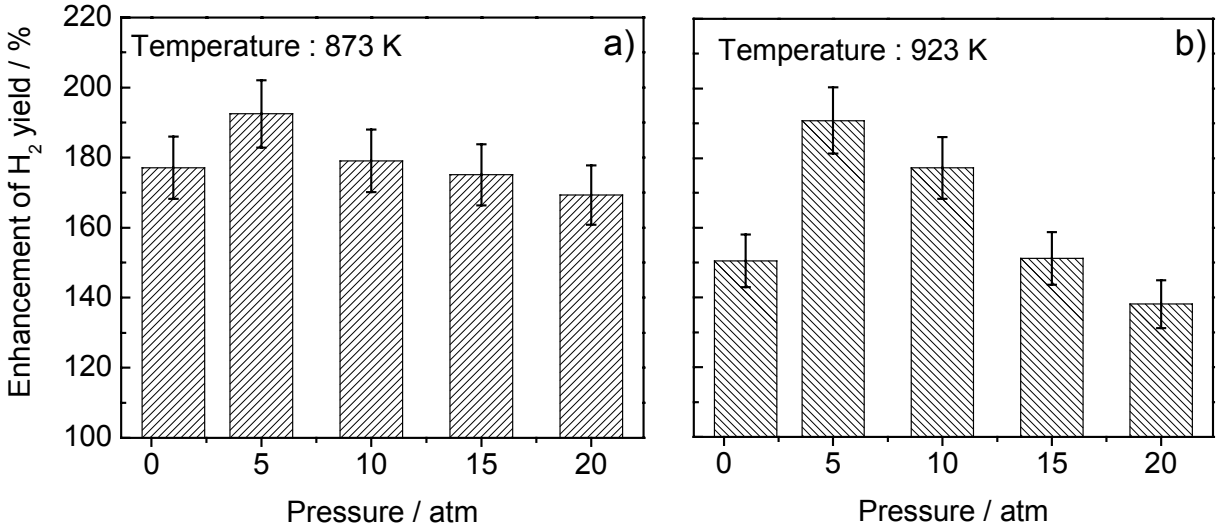

Figure 5.11. Enhancements in the H_2 yield in the MR compared to PFR at various pressures. ($Enhancement\ (\%) = \frac{Yield\ \ (MR)}{Yield\ \ (PFR)} \times 100$)

The yields of CO achieved in the MR were also significantly higher than the yields obtained in the PBR. The enhancements in the yields of CO in the MR are shown versus pressure in Figures 5.12a) and 5.12b). At 873 K the enhancement of the CO yields reached a maximum at 5 atm, where the yield achieved in the MR was about 130 % higher than that obtained in the PBR. Similar behavior was observed at 923 K with the enhancement again showing a maximum at 5 atm, with a yield in the MR about 125 % higher than in the PBR.

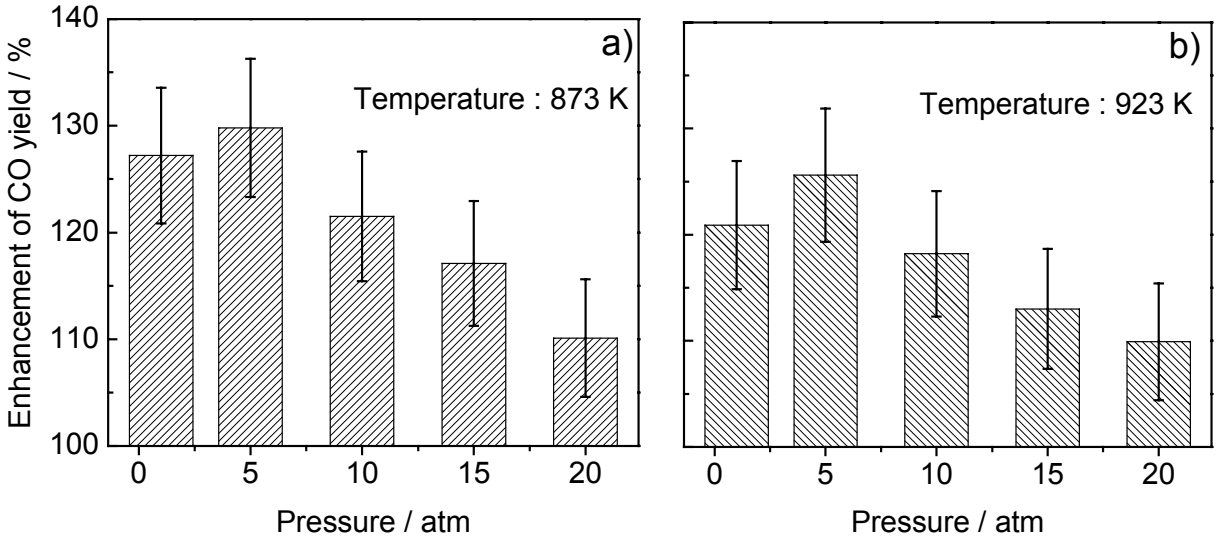

Figure 5.12. Enhancement of CO yield in the MR vs. reaction pressure

In summary, the results of the enhancements in the yields of CO and H_2 presented above indicated that higher yields were achieved in the MR compared to the PBR. The yields of both CO and H_2 showed a maximum enhancement in the MR at 5 atm at both 873 K and 923 K. This was consistent with the results for the hydrogen separation shown in Figures 5.10a) and 5.10b), where the maximum hydrogen separation was obtained in the MR at 5 atm. These results clearly show that the enhancements in the yields of both CO and H_2 were due to the concurrent removal of the product hydrogen from the reaction in the MR. The results also indicated that high enhancements in both CO and H_2 yields in the MR can be obtained when the hydrogen removal from the reaction system is high. From a kinetic point of view, the RWGS reaction is very fast and reached equilibrium in the PBR while the reforming reaction operated below equilibrium in this work. A significant aspect of this study was the investigation of the effect of pressure in a membrane reactor using a reaction with an increase in moles. It was found that as pressure increased the yield of hydrogen increased, passed through a maximum where the separation of the hydrogen from the reaction was the highest, and then decreased. This result was a consequence of a tradeoff between increased permeability with pressure balanced by decreasing equilibrium production of hydrogen due to thermodynamics. This is the first time such a trade-off has been documented in the membrane reactor literature.

5.5. Conclusions

The dry-reforming of methane ($CH_4 + CO_2 \rightleftharpoons 2\ CO + 2\ H_2$) was studied in a membrane reactor (MR) with a hydrogen-selective ceramic membrane at various pressures and temperatures and the results were compared to those obtained in a packed-bed reactor (PBR) of the same geometry. It was found that the concurrent and selective removal of hydrogen from the reaction in the MR resulted in significant improvement over the PBR in the yields of the reaction products, CO and H_2, with levels exceeding equilibrium sometimes obtained.

Pressure had a substantial effect on the performance of the membrane reactor. Because of the increase in the number of moles in the dry-reforming reaction, the production of H_2 was not favored at high pressures. However, hydrogen permeability through the membrane increased with pressure. As a consequence the yield of hydrogen in the membrane reactor at first rose with pressure because of increasing permeability, but then dropped because of the unfavorable

equilibrium and enhanced rate of the reverse reaction. This result indicated that pressure caused a tradeoff between thermodynamic and kinetic quantities.

The reverse water gas shift reaction was found to have a serious impact in the operation of the dry-reforming reaction. Although its effect was minimal at atmospheric pressure, at high pressures the suppression of the dry-reforming reaction caused much of the hydrogen produced to be converted to water. The use of the MR alleviated the situation but did not solve the problem.

References

[i] D.W. Breck, Zeolite Molecular Sieves: Structure, Chemistry and Use, Wiley, New York, 1974, p.636.

[ii] Richardson, J. T.; Paripatyadar, S. A. Carbon dioxide reforming of methane with supported rhodium. *Appl. Catal.* **1990**, 61, 293.

[iii] Bradford, M. C.; Vannice, M. A. CO_2 reforming of CH_4. *Catal. Rev.-Sci.Eng.* **1999**, 41, 1.